Dalton Transactions

ROYAL SOCIETY OF CHEMISTRY

PAPER

View Article Online
View Journal | View Issue

Cite this: *Dalton Trans.*, 2026, **55**, 6035

Phosphorescence properties of boron β-diketiminate complexes modulated by spiro structures

Keisuke Suwa,[a] Shunichiro Ito [a,b] and Kazuo Tanaka *[a,b]

Received 17th February 2026,
Accepted 17th March 2026

DOI: 10.1039/d6dt00417b

rsc.li/dalton

Comprehension of the photochemical properties of triplet excited states in organic compounds is of significance for developing advanced organic light-emitting devices, organic photocatalysts, and luminescent probes. However, triplet excited states of typical organic chromophores without heavy atoms are hard to generate because intersystem crossing from singlet to triplet excited states is spin-forbidden. Recently, we demonstrated that efficient crystallization-induced room-temperature phosphorescence is observed in β-diketiminate complexes of group 13 elements bearing heavy halogen substituents on the central atom. In this research, to obtain phosphorescence from β-diketiminate complexes without the use of heavy atoms, twisted donor–acceptor systems were constructed on a central atom through a spiro structure. The resulting biphenylene-based β-diketiminate boron complexes exhibited phosphorescence even at room temperature. On the other hand, diolate-based spiro complexes exhibited only inefficient room-temperature emission. Theoretical calculations suggested that interligand charge-transfer states provided by the spiro structure should facilitate efficient intersystem crossing. In addition, the moderately electron-donating properties of the biphenylene units should be responsible for the room-temperature phosphorescence.

Introduction

Organic compounds that emit *via* triplet excited states, such as phosphorescence and thermally activated delayed fluorescence, have been extensively developed to achieve efficient organic light-emitting diodes[1,2] and luminescent probes.[3] Additionally, triplet excited states of organic compounds have been thoroughly studied to realize efficient photoredox catalysts and energy conversion/harvesting materials.[4,5] Therefore, tremendous efforts have been devoted to developing novel scaffolds with unique electronic properties regarding triplet excited states.[6–11] In this context, a common issue with typical organic molecules is their difficulty in generating triplet excited states, because the transitions from singlet to triplet excited states, *i.e.*, intersystem crossing (ISC), are spin-forbidden. This phenomenon arises from the selection rule that a transition involving a change in total angular momentum ($\Delta J = \Delta L + \Delta S$, where ΔL and ΔS are the changes in the orbital and spin angular momenta, respectively) is forbidden. Introducing heavy metals such as platinum and iridium into molecular structures accelerates ISC and leads to efficient phosphorescence, a phenomenon known as the heavy-atom effect. However, methods to achieve rapid ISC and emissions *via* triplet states without relying on heavy metals remain highly desirable to address the high cost and potential toxicity of heavy metals.

Another way to obtain fast ISC is based on the El-Sayed rule, originally developed for carbonyl compounds.[12,13] Carbonyl compounds like acetophenone often show dramatically fast ISC (ISC rate constant, $k_{ISC} \sim 10^{10}$ s^{-1}) because the dominant ISC process, consisting of the S(nπ*)–T(ππ*) transition, involves non-zero ΔL. In this transition, the spin–flip occurs along with a non-zero ΔL, resulting in $\Delta J = 0$, induced by spin–orbit coupling (SOC). Consequently, this S–T transition is no longer forbidden. Although this mechanism does not involve heavy atoms, it has not been utilized for constructing luminescent materials because carbonyl compounds hardly emit due to the nπ* character of their lowest excited states (S_1 and T_1).

Twisted donor–acceptor structures, in which the donor and acceptor units are directly bonded but the π-conjugation system is twisted, can often exhibit fast ISC and efficient phosphorescence without heavy atoms.[14–16] The twisted conformation provides non-zero ΔL during ISC from a charge transfer (CT) state to a locally excited (LE) state, and *vice versa*. Indeed, we recently demonstrated that β-diketiminate (DKI)

[a]*Department of Polymer Chemistry, Graduate School of Engineering, Kyoto University, Nishikyo-ku, Katsura, Kyoto 615-8510, Japan.*
E-mail: tanaka@poly.synchem.kyoto-u.ac.jp
[b]*Department of Technology and Ecology, Graduate School of Global Environmental Studies, Kyoto University, Katsura, Nishikyo-ku, Kyoto 615-8510, Japan*

complexes of group 13 elements exhibit dual emission bands consisting of fluorescence and phosphorescence at 77 K in solution.[17–25] Therefore, it is presumable that the DKI complexes involving twisted structures might be a potential platform for expressing unique optical properties concerning triplet excited states in the absence of heavy atoms.

Herein, we report the synthesis and electronic properties of boron DKI complexes with a spiro structure. Boron-based donor–spiro–acceptor type systems have recently been developed as functional dyes with thermally activated delayed fluorescence and/or singlet-oxygen photosensitizing ability.[26–31] Therefore, we designed a new molecular system in which the tetracoordinate boron atom is fixed in a vertical conformation between the BN_2C_3 ring of DKI ligands and the biphenylene and diolate substituents, serving as an electron donor. We found that photoluminescence properties depend strongly on the type of donor. Additionally, it is clearly shown that the biphenylene complexes exhibit room-temperature phosphorescence (RTP) in their crystalline states.

Results and discussion

Synthesis and characterization

The chemical structures and synthesis of the spiro boron complexes with DKI ligands are shown in Scheme 1. For the biphenylene compounds, phenyl and mesityl groups were employed as the aryl units in the DKI ligands, because the different substituents should differ in intermolecular interactions and lead to a change in solid-state luminescence properties. The bromine atoms in **Ph_FLBr** were introduced to alter intermolecular interactions and employ the heavy-atom effect, which usually accelerates ISC processes. For the diolate compounds, catechol and 2,3-naphthalenediol were used as donors with different orbital energies.

The DKI ligands were synthesized by the reaction of *N*-phenylimine and imidoyl chloride with their respective substituents. Biphenylene complexes, **Mes_FL**, **Ph_FL**, and **Ph_FLBr**, were prepared through the reaction of the ligands with *n*-butyllithium and subsequently the corresponding 9-halo-9-borafluorene derivatives. Diolate complexes, **Mes_cat** and **Mes_naph**, were prepared by the treatment of **Mes_L** with boron tribromide in dichloromethane, followed by reaction with the respective diolates in toluene. All compounds were fully characterized using ^{1}H and $^{13}C\{^{1}H\}$ NMR spectroscopy and high-resolution mass spectrometry. Additionally, the boron complexes were characterized by $^{11}B\{^{1}H\}$ NMR spectroscopy and single-crystal X-ray structure analysis. The detailed procedures and characterization data are provided in the SI.

The crystal structures of the synthesized compounds are shown in Fig. 1 and S1. The crystals of **Mes_FL** and **Ph_FLBr** contain crystal solvents of hexane (complex : solvent = 1 : 0.5) and chloroform (complex : solvent = 1 : 1), respectively. Importantly, there was no apparent π–π stacking in all crystals, probably because of the sterically encumbered ligands and the

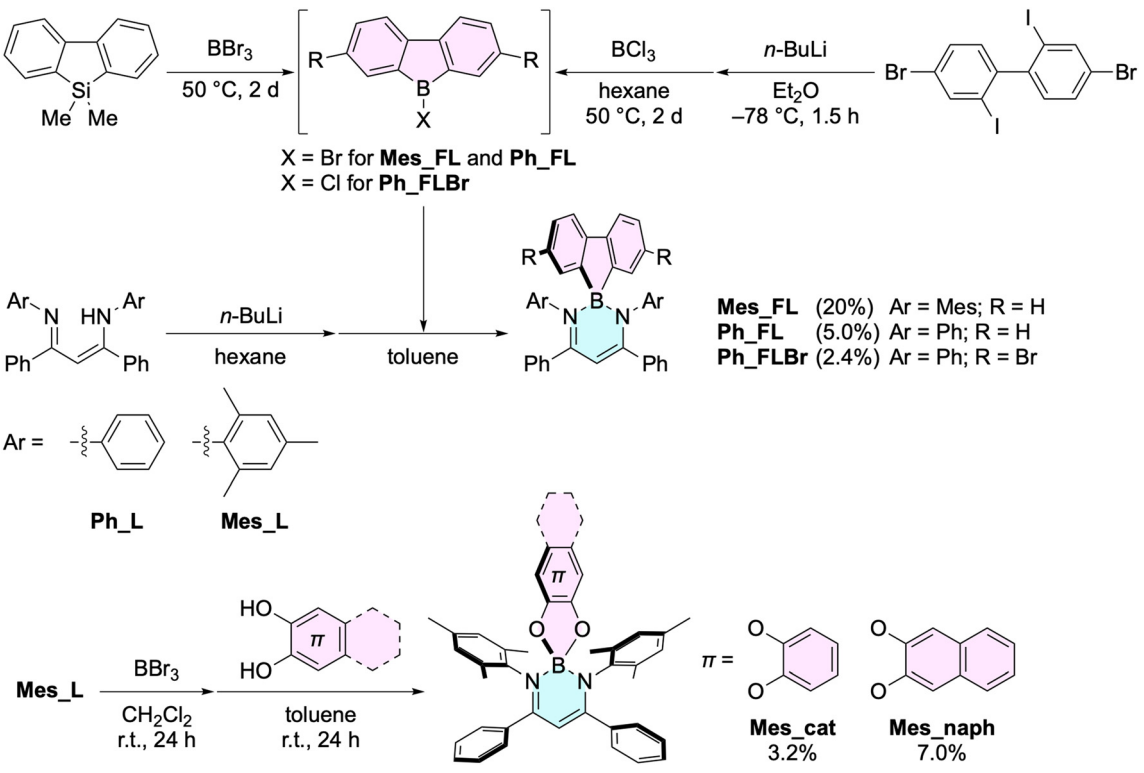

Scheme 1 Synthetic scheme of biphenylene, diolate, and diphenyl boron complexes.

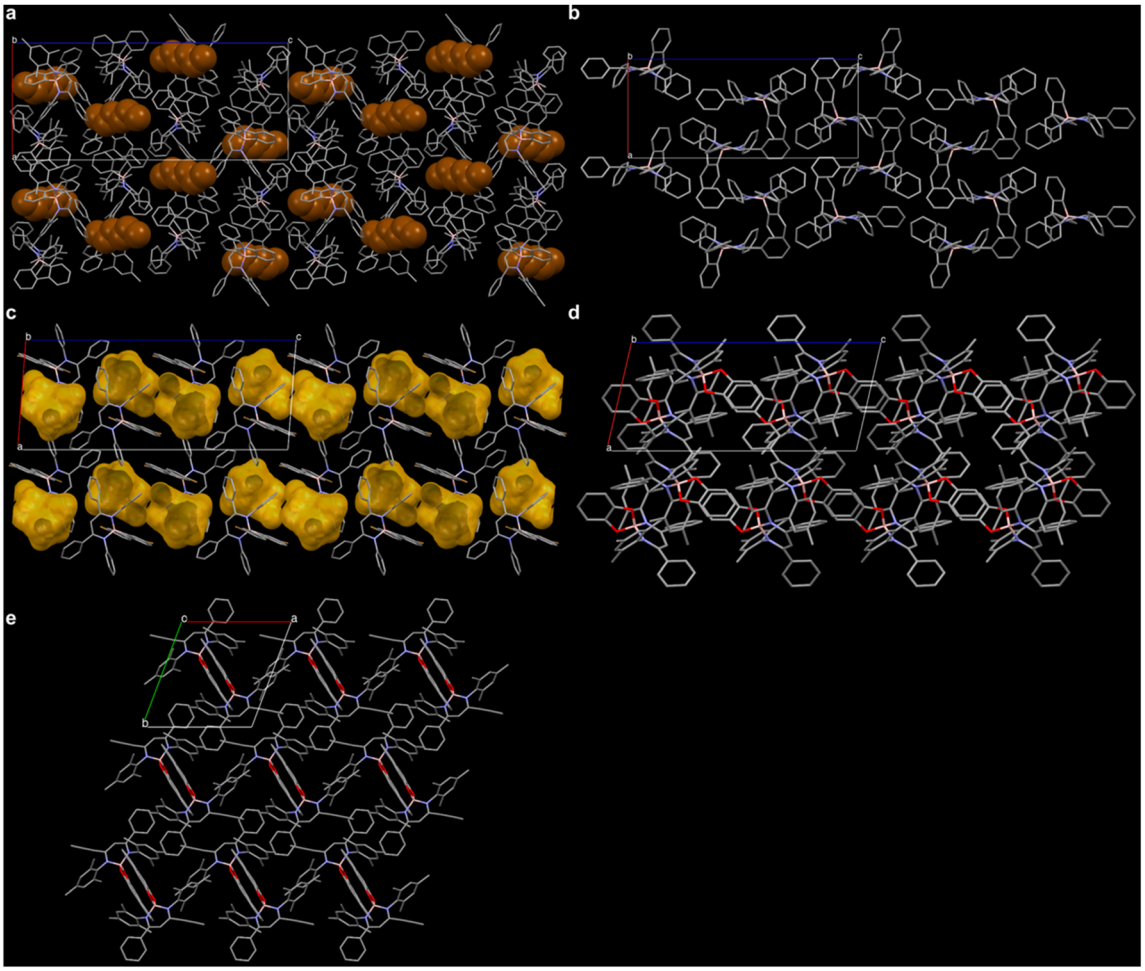

Fig. 1 Packing structures of (a) **Mes_FL**, (b) **Ph_FL**, (c) **Ph_FLBr**, (d) **Mes_cat**, and (e) **Mes_naph**. In (a), hexane molecules in the crystal of **Mes_FL** are shown in brown. In (c), solvent sites occupied by chloroform are depicted as yellow surfaces, which are calculated as a contact surface on Mercury 2023.3.1 (probe radius = 1.2 Å; approximate grid spacing = 0.3 Å).

spiro structures. Therefore, the electronic structures of the single molecules might not be strongly modulated by intermolecular interactions.

Photophysical properties of biphenylene complexes

The biphenylene complexes exhibited clear crystallization-induced emission at room temperature. The crystalline samples exhibited greenish-yellow emission under UV irradiation (365 nm) at room temperature, while their dilute solutions (2-methyltetrahydrofuran (2MeTHF), 1×10^{-5} M) showed almost no emission at the same temperature. In the absorption spectra of all compounds, the large absorption bands were shown in the visible region (Fig. 2 and Table 1; 431–443 nm). In 2MeTHF at room temperature, emission was hardly observed. In stark contrast to the solutions, the crystalline samples showed significantly stronger emission in the 524–556 nm wavelength range (Fig. 2). Moreover, the absolute PL quantum yields (Φ_{PL}) of these crystals were dramatically higher (up to 0.38 for **Ph_FLBr**) than those of the solutions (<0.01). PL lifetime measurements of the crystals revealed that these emission bands have nanosecond lifetimes and are therefore primarily fluorescence (Table S1).

Interestingly, in PL spectra recorded with a 0.1 ms delay after photoexcitation, a longer-wavelength delayed emission was observed from their crystals (Fig. 2). The PL lifetime of the delayed component of **Mes_FL** was estimated to be approximately 2 ms (Table S2), suggesting the RTP properties. The phosphorescence quantum yield of **Ph_FLBr**, estimated from the integration ratio, was comparable with that of the others (Table 1). Consequently, the fluorescence quantum yield of **Ph_FLBr** was much higher than that of the others. As this fluorescence enhancement seems contrary to the usual heavy-atom effect, it was suggested that the bromine atoms at the biphenylene unit might not significantly accelerate the ISC process.

According to the previous studies, the phosphorescence from DKI complexes of group 13 elements was observed only at low temperatures,[17,18,20,21,23,24] except for dibromo- and diiodoaluminum complexes.[25] In these previous cases, it was suggested that the fast ISC could proceed from the S_1 state with a locally excited (LE) character to the T_n state with an

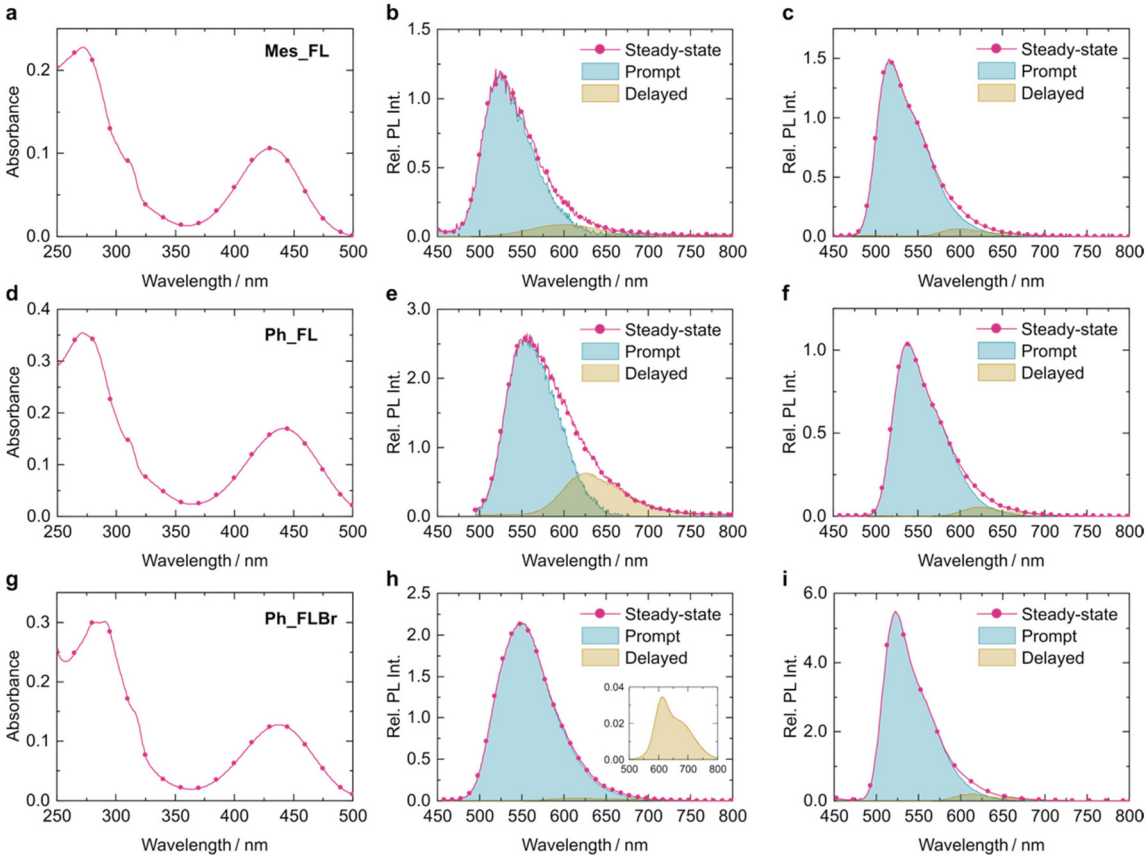

Fig. 2 (a, d and g) UV–vis absorption spectra in 2MeTHF at room temperature, (b, e and h) PL spectra in crystalline states at room temperature, and (c, f and i) PL spectra in 2MeTHF (1×10^{-5} M) at 77 K for (a–c) **Mes_FL**, (d–f) **Ph_FL**, and (g–i) **Ph_FLBr**. Delayed PL spectra were recorded 0.1 ms after pulse photoexcitation. Prompt PL spectra were calculated by subtraction of a delayed spectrum from a steady-state spectrum. Inset in (h): enlarged spectrum of the delayed component.

Table 1 Optical properties of biphenylene complexes at room temperature

	Solution[a]	Crystal[b]				
	λ_{abs} [c]/nm	λ_{em}^{SS} [d,e]/nm	$\lambda_{em}^{Delayed}$ [d,f]/nm	Φ_{PL}^{Total} [d,g]	Φ_{PL}^{Prompt} [h]	$\Phi_{PL}^{Delayed}$ [h]
Mes_FL	431	524	587	0.02	0.02	<0.01
Ph_FL	443	556	627	0.10	0.09	0.01
Ph_FLBr	438	550	607	0.38	0.37	0.01

[a] 2MeTHF solution (1×10^{-5} M). [b] Recrystallized from $CHCl_3$ or CH_2Cl_2–hexane. [c] Wavelength at the absorption maximum in the visible region. [d] Excited at λ_{abs}. [e] Wavelength at the steady-state PL maximum. [f] Wavelength at the delayed PL maximum detected with a 0.1 ms delay after excitation. [g] Absolute PL quantum yield. [h] Relative quantum yields for prompt (Φ_{PL}^{Prompt}) and delayed ($\Phi_{PL}^{Delayed}$) components estimated from the integration ratio ($\Phi_{PL}^{Total} = \Phi_{PL}^{Prompt} + \Phi_{PL}^{Delayed}$).

intraligand CT character within the DKI ligands.[24,25] On the other hand, the phosphorescence of the biphenylene complexes in this work was observed even at room temperature, implying contributions from other mechanisms.

To evaluate the electronic structures at the single molecule level without significant molecular motion, we measured PL spectra in 2MeTHF solutions at 77 K (Fig. 2). **Mes_FL**, **Ph_FL**, and **Ph_FLBr** showed remarkably intense fluorescence at 516–537 nm and a phosphorescence component at 598–623 nm. The quantum yields of phosphorescence were still lower (0.02–0.03) than those of fluorescence (0.35–0.72; Table 2). These fluorescence-rich emissions, even at 77 K, also contrast with those of the previously reported group 13 DKI complexes, which typically exhibit a clearly bimodal dual emission of fluorescence and phosphorescence under the same conditions.[17,18,20,21,23,24]

Photophysical properties of diolate complexes

In contrast to the biphenylene complexes, the emission from diolate complexes was below the detection limit at room temp-

Table 2 Optical properties of fused complexes in solution at 77 K [a]

	λ_{em}^{SS} [b,c]/nm	$\lambda_{em}^{Delayed}$ [b,d]/nm	Φ_{PL}^{Total} [b,e]	Φ_{PL}^{Prompt} [f]	$\Phi_{PL}^{Delayed}$ [f]
Mes_FL	516	598	0.37	0.35	0.02
Ph_FL	537	623	0.44	0.41	0.03
Ph_FLBr	523	613	0.75	0.72	0.03

[a] In 2MeTHF (1×10^{-5} M). [b] Excited at λ_{abs}. [c] Wavelength at the steady-state PL maximum. [d] Wavelength at the delayed PL maximum detected with a 0.1 ms delay after excitation. [e] Absolute PL quantum yield. [f] Relative quantum yields for prompt (Φ_{PL}^{Prompt}) and delayed ($\Phi_{PL}^{Delayed}$) components estimated from the integration ratio ($\Phi_{PL}^{Total} = \Phi_{PL}^{Prompt} + \Phi_{PL}^{Delayed}$).

erature in both solution and crystalline states. On the other hand, the complexes showed green emission at 77 K in solution. Their photophysical properties were investigated with UV–vis absorption and PL spectra at 77 K (Fig. 3 and Table 3). In both compounds, intense absorption bands were observed in the UV region, with a peak around 360 nm in EPA (EtOH/isopentane/Et_2O = 2/5/5 (v/v/v)). In 77 K solutions, significantly, **Mes_cat** showed a weak bimodal emission peaking at 414 and 494 nm, whereas **Mes_naph** exhibited an intense unimodal emission at 494 nm with a vibrational structure. Lifetime measurements revealed that each emission band at 494 nm of both compounds should be attributed to phosphorescence because of their millisecond lifetimes (117 ms for **Mes_cat**; 140 ms for **Mes_naph**). Meanwhile, the emission band of **Mes_cat** around 414 nm was attributable to fluorescence, as evidenced by its short lifetime, which was not determined due to the low intensity. Such long-lifetime phosphorescence at 77 K is consistent with the previous results on DKI complexes of group 13 elements.[18] It should be noted that the phosphorescence quantum yield of **Mes_naph** (0.05) was higher than that of **Mes_cat** (<0.01) but lower than that of representative DKI complexes (up to approximately 0.95).[21,24,25,32] These results indicate that the diolate substituents affect the electronic properties of DKI complexes in a different manner than biphenylenes.

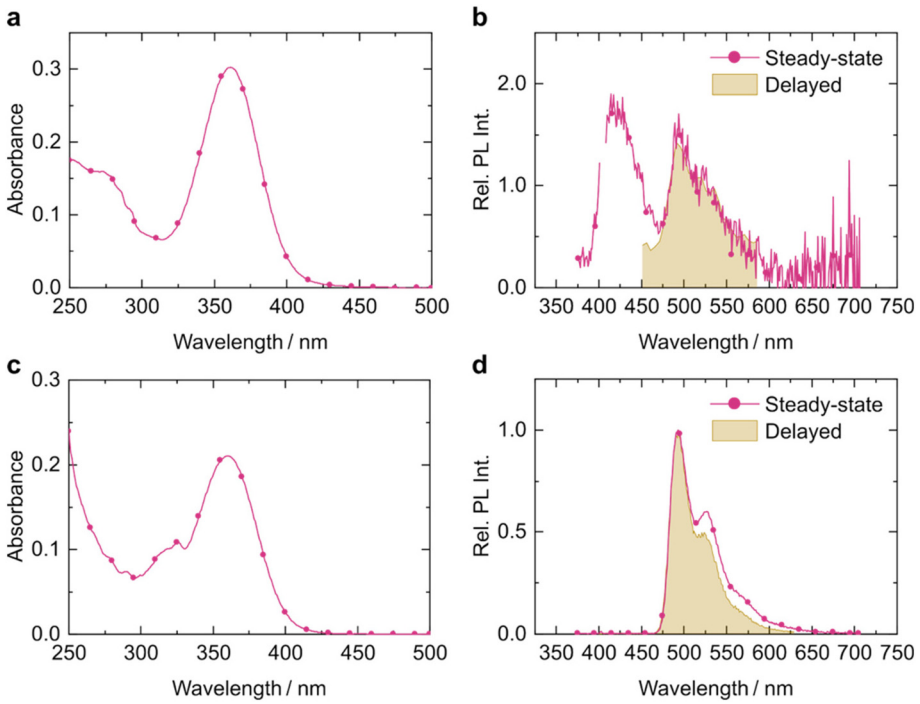

Fig. 3 (a and c) UV–vis absorption spectra at room temperature and (b and d) PL spectra at 77 K for (a and b) **Mes_cat** and (c and d) **Mes_naph** in EPA (1×10^{-5} M). Delayed PL spectra were recorded 0.1 ms after pulse photoexcitation.

Table 3 Optical properties of diolate complexes in solution[a]

	λ_{abs} [b]/nm	$\lambda_{em,\ FL}$ [c]/nm	$\lambda_{em,\ Phos}$ [c]/nm	$\Phi_{PL,\ all}$ [c,d]	$\Phi_{PL,\ FL}$ [c,e]	$\Phi_{PL,\ Phos}$ [c,e]
Mes_cat	361	414	494	<0.01	<0.01	<0.01
Mes_naph	360	—[d]	494	0.05	—[d]	0.05

[a] In EPA (1×10^{-5} M). [b] Measured at room temperature. [c] Measured at 77 K. [d] Absolute PL quantum yield measured by the integrating sphere method. Excited at λ_{abs}. [e] Estimated by calculating the integration ratios of fluorescence and phosphorescence bands in the steady-state spectrum.

Kinetics of photophysical processes

To obtain further information on the photophysical properties of the biphenylene complexes, rate constants for each photophysical process were estimated from PL quantum yields and lifetimes (Table S3). In the crystalline state, the fluorescence rate constant (k_{FL}) of **Ph_FLBr** (1.2×10^8 s^{-1}) was much larger than that of the other complexes (5.7×10^7 s^{-1} for **Mes_FL**; 8.8×10^7 s^{-1} for **Ph_FL**). Meanwhile, the rate constant of the non-radiative decay from the singlet excited state (k_{nr}^S), which involves internal conversion and ISC processes, varied in the order of **Mes_FL** (3.6×10^8 s^{-1}) > **Ph_FL** (5.8×10^7 s^{-1}) > **Ph_FLBr** (9.3×10^6 s^{-1}). Typical DKI complexes undergo drastic structural changes in the excited state, forming folded structures with a twisted C–N bond in the EN_2C_3 ring (E = group 13 element). In these structures, k_{FL} and k_{nr}^S are small and large, respectively, because they should be near or form a conical intersection.[25] Therefore, such an electronic state with a folded structure can be stated as a dark state.

It is assumed that **Mes_FL** is most prone to accessing the dark state, even in the crystalline powder sample. Indeed, the SCXRD analysis revealed that the **Mes_FL** crystal grown from a hexane solution contains solvent sites occupied by hexane molecules (Fig. 1a; **Mes_FL** : hexane = 1 : 0.5). In addition, the powder X-ray diffraction pattern for the crystalline powder used for the photophysical measurements well matched the profile predicted from the SCXRD results (Fig. S2). On the other hand, the ^{1}H NMR spectrum for the same crystalline powder showed only a small amount of hexane (Chart S11). These observations suggest that the crystalline powder should contain voids in the packing and that the **Mes_FL** molecules have the highest movability in the crystalline states among the biphenylene complexes. In contrast, although the single crystal structure of **Ph_FLBr** also contains solvent molecules, NMR and powder X-ray diffraction measurements suggest that the crystalline sample for optical measurements possessed a different crystal structure without any solvent molecules. Consequently, access to the dark state in **Ph_FLBr** might be restricted. Therefore, the smallest k_{nr}^S value should be obtained from **Ph_FLBr**. Unfortunately, the PL lifetimes of the diolate complexes have not been determined because of their low PL intensity.

Theoretical calculations

To evaluate the electronic structures of the biphenylene complexes, density functional theory (DFT) and time-dependent DFT (TD-DFT) calculations with the Tamm–Dancoff approximation (TDA) were performed. Geometry optimization and single-point energy calculations were carried out at the CAM-B3LYP/6-31+G(d,p) and the unrestricted CAM-B3LYP/6-311++G(d,p) levels of theory, respectively. In addition, natural transition orbital (NTO) calculations were performed to evaluate the excited-state electronic structures. Calculation details are shown in the SI.

Fig. 4a shows the calculated energy diagrams of the complexes with S_0-optimized geometries. For the biphenylene complexes, the highest-occupied and lowest-unoccupied NTOs (HOTO and LUTO) of their S_1 states are localized on the DKI moieties (Fig. 4b and S4–S6), indicating LE character centered on the DKI unit (LE(DKI)). As a result, the oscillator strengths (f) for the S_0–S_1 transition were comparable (Fig. 4a). Therefore, the differences in PL behavior and the RTP properties of the biphenylene complexes should mainly originate from excited-state dynamics involving ISC and structural relaxations. Unfortunately, the S_1 structure optimizations did not converge, likely due to the presence of conical intersections. Therefore, the effects of structural relaxations have not been evaluated. Meanwhile, significant structural deformations could be restricted in the solid states or at 77 K. Consequently, the properties of the complexes were studied based on the S_0-optimized structures.

For assessing ISC properties, the SOC constants between S_1 and T_n states ($\xi(S_1$–$T_n)$) were calculated (Table 4, see the SI). It was reported that ISC processes from S_1 to higher triplet states can occur at room temperature when the S_1–T_n energy gap is within ± *ca.* 0.3 eV, even if the transition is uphill.[5] The number of triplet states near the S_1 state within this energy range is similar among the biphenylene complexes (T_2–T_4 states; Fig. 4a). Thus, the ISC in the biphenylene complexes should smoothly occur even at room temperature because of their prominent $\xi(S_1$–$T_n)$ values (>1, Table 4). Consequently, phosphorescence from the biphenylene complexes can be observed even at room temperature.

The NTO analysis revealed that the T_n (n = 2–4) states of the biphenylene complexes are mainly composed of the following transitions (Fig. 4b and S4–S6): LE(FL), local excitation centered on the borafluorene unit; intra-LCT(Ph → DKI), intraligand CT excitation from the peripheral phenyl or mesityl rings to the central BN_2C_3 ring; inter-LCT(FL → DKI), interligand CT excitation from the borafluorene unit to the central BN_2C_3 ring. As the FL and the peripheral aromatic rings are connected to the central BN_2C_3 ring with substantial dihedral angles, the S_1–T_n transitions should proceed with non-zero ΔL, leading to significantly large $\xi(S_1$–$T_n)$ values. The additional ISC channels provided by the FL unit could be responsible for the RTP properties of the biphenylene complexes, which are absent in the difluoroboron complexes.[17,18] In addition, the possible reason why the bromine atoms hardly enhance phosphorescence might stem from the only small contribution of the bromine atoms to the HOTO and LUTO for the excited states (Fig. S5).

Fig. 4a also shows the energy diagrams for the diolate complexes. The S_1 states of both complexes have negligible oscillator strengths, in contrast to those of the biphenylene complexes. This could be the origin of their significantly inefficient luminescence. The NTO analysis reveals that the S_1 state of the diolate complexes should be attributed to the inter-LCT (diol → DKI) transition (Fig. 4c and S6–S8). The negligible overlap between the HOTO and LUTO should result in small f values. The strong electron-donating ability of the diolate ligands should provide a higher-lying HOMO, leading to the inter-LCT state as their S_1 state. On the other hand, the S_2 state of

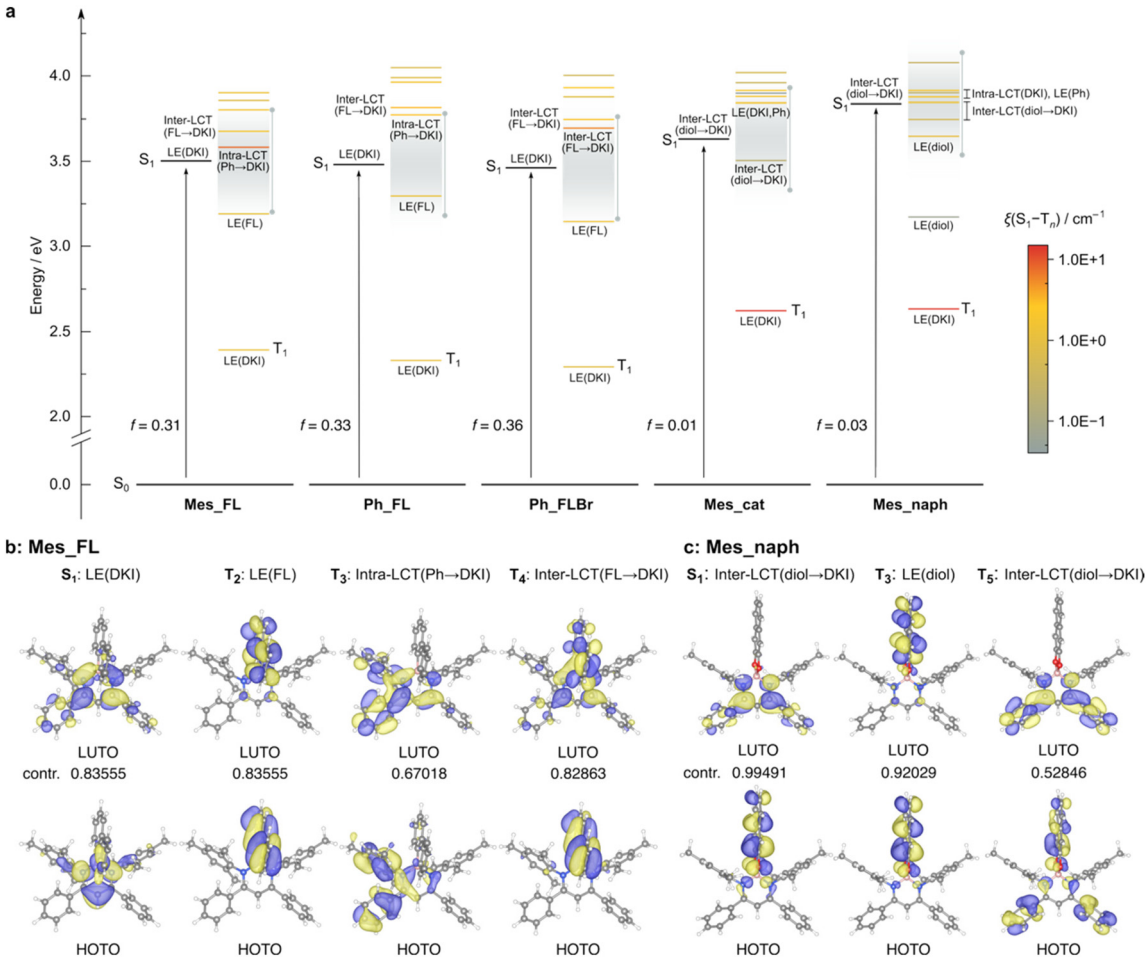

Fig. 4 (a) Electronic state energy diagrams of singlet and triplet levels at the TDA-UCAM-B3LYP/6-311++G(d,p) level of theory. *f* denotes the oscillator strength for the S_0–S_1 transition. The color of the bars for triplet states corresponds to the $\xi(S_1–T_n)$ values on the color scale. Grey vertical bars show the range of ±0.3 eV from the S_1 state. Selected NTOs of (b) **Mes_FL** and (c) **Mes_naph**. Contr. represents the contribution of the NTO pair to the corresponding electronic transition. NTOs were visualized using VESTA.[33]

Table 4 Calculated electronic transition energies and SOC constants between S_1 and T_n states

		T_1	T_2	T_3	T_4	T_5	T_6	T_7	T_8	T_9
Mes_FL	Energy/eV	2.39	3.19	3.58	3.68	3.80	3.86	3.90	4.06	4.13
	$\xi(S_1–T_n)/cm^{-1}$	1.06	1.14	7.52	1.61	1.76	0.75	1.30	—[a]	—[a]
Ph_FL	Energy/eV	2.33	3.30	3.77	3.82	3.96	3.99	4.05	4.11	4.27
	$\xi(S_1–T_n)/cm^{-1}$	0.86	1.13	2.70	3.21	1.67	0.81	0.55	—[a]	—[a]
Ph_FLBr	Energy/eV	2.29	3.15	3.69	3.75	3.88	3.93	4.00	4.01	4.19
	$\xi(S_1–T_n)/cm^{-1}$	0.85	1.21	5.67	2.70	0.84	1.78	0.39	—[a]	—[a]
Mes_cat	Energy/eV	2.62	3.51	3.84	3.88	3.90	3.92	3.96	4.02	4.39
	$\xi(S_1–T_n)/cm^{-1}$	13.05	0.19	1.53	1.67	0.05	1.88	0.38	0.52	—[a]
Mes_naph	Energy/eV	2.63	3.17	3.65	3.75	3.84	3.88	3.90	3.92	4.08
	$\xi(S_1–T_n)/cm^{-1}$	12.91	0.06	0.97	0.46	1.31	1.73	0.27	1.76	0.30

[a] Not calculated.

Mes_cat and the S_3 state of **Mes_naph** are attributed to the LE (DKI) state. Their considerable oscillator strengths should be responsible for the absorption bands in the visible region.

Importantly, there are more triplet excited states near the S_1 state of **Mes_naph** than that of **Mes_cat** (Fig. 4a). In addition, the NTO analysis revealed that the T_2 state of **Mes_cat** is attributable to the inter-LCT (diol → DKI) transition, as in its S_1 state. Therefore, the transition between S_1 and T_2 involves only a small ΔL, resulting in a small $\xi(S_1–T_2)$ value (0.19 cm^{-1}). Meanwhile, the T_3–T_6 states of **Mes_naph** are mainly com-

posed of the LE(diol), inter-LCT(diol → DKI), intra-LCT(Ph → DKI), and LE(Ph) transitions (Fig. 4c and S6–S8). Consequently, the S_1–T_n (n = 3–6) transitions could involve a substantial ΔL, leading to relatively large $\xi(S_1\text{–}T_n)$ values (Table 4). These results strongly suggest that the ISC process of **Mes_naph** should be faster than that of **Mes_cat**. As a result, the phosphorescence quantum yield of **Mes_naph** was higher, and fluorescence was hardly observed from **Mes_naph**.

Furthermore, the diolate complexes showed little emission at room temperature, whereas the biphenylene complexes exhibited both phosphorescence and fluorescence. This stark difference could be explained by the following mechanism: the S_1 state of diolate complexes was composed of the inter-LCT (diol → DKI) transition, with negligible f, resulting in a small k_{FL}. On the other hand, the S_1 state of the biphenylene complexes was attributed to the LE(DKI) transitions with large f, leading to large k_{FL}, similar to typical DKI complexes (Fig. 4).[1,3] The corresponding LE(DKI) states of the diolate complexes are located in the higher energy region (S_2 of **Mes_cat** and S_3 of **Mes_naph**). The occupied orbital of the DKI unit is stabilized and destabilized by the inductively electron-withdrawing diolate units and the σ-donating biphenylene units, respectively. Meanwhile, the energy of the unoccupied orbital is not significantly affected by the substituents on the boron atom (Fig. S9). As a result, the LE states of the diolate complexes localized at the DKI unit are located at a higher energy region than those of the biphenylene complexes (Table S7).

Conclusion

We synthesized a new series of DKI boron complexes with a spiro structure at the boron center. Importantly, it is demonstrated that their excited-state properties, involving ISC and phosphorescence processes, are significantly tunable by modulating the electronic properties of the substituents connected to the boron atom with a spiro configuration. Particularly, the biphenylene complexes exhibited room-temperature phosphorescence derived from accelerated ISC through higher-lying excited triplet states. The design concept for introducing a spiro structure at the coordination center could be applicable to the development of not only novel luminescent complexes but also other functional dyes, such as organic photoredox catalysts.

Conflicts of interest

The authors declare no competing interests.

Data availability

The data supporting this article have been included as part of the supplementary information (SI). Supplementary information is available. See DOI: https://doi.org/10.1039/d6dt00417b.

CCDC 2529534–2529538 contain the supplementary crystallographic data for this paper.[34a–e]

Acknowledgements

This work was partially supported by a Grant-in-Aid for Early-Career Scientists (for S. I., JSPS KAKENHI Grant Number: 23K13793) and for Scientific Research (B) (for K. T., JSPS KAKENHI Grant Number: 24K01570) and the National Research Foundation of Korea (NRF) grant funded by the Korean government (MSIT) (No. RS-2024-00406152).

References

1 C. Adachi, M. A. Baldo, M. E. Thompson and S. R. Forrest, *J. Appl. Phys.*, 2001, **90**, 5048–5051.
2 H. Uoyama, K. Goushi, K. Shizu, H. Nomura and C. Adachi, *Nature*, 2012, **492**, 234–238.
3 J. Chen, H. Lan, S. Zhou, W. Chen, X. Zhen and X. Jiang, *Aggregate*, 2026, **7**, e70243.
4 S. Fukuzumi, H. Kotani, K. Ohkubo, S. Ogo, N. V. Tkachenko and H. Lemmetyinen, *J. Am. Chem. Soc.*, 2004, **126**, 1600–1601.
5 N. A. Romero and D. A. Nicewicz, *Chem. Rev.*, 2016, **116**, 10075–10166.
6 T. Hatakeyama, K. Shiren, K. Nakajima, S. Nomura, S. Nakatsuka, K. Kinoshita, J. Ni, Y. Ono and T. Ikuta, *Adv. Mater.*, 2016, **28**, 2777–2781.
7 Y. Tani, K. Miyata, E. Ou, Y. Oshima, M. Komura, M. Terasaki, S. Kimura, T. Ehara, K. Kubo, K. Onda and T. Ogawa, *Chem. Sci.*, 2024, **15**, 10784–10793.
8 X. Zou, N. Gan, Y. Gao, L. Gu and W. Huang, *Angew. Chem., Int. Ed.*, 2025, **64**, e202417906.
9 Z. Yin, Z. Wu and B. Liu, *Adv. Mater.*, 2025, **37**, e2506549.
10 W. Huang, C. Wei, Y. Zhu, Q. Zhang and Z. He, *Chem. Sci.*, 2025, **17**, 956–967.
11 X. Long, Z. Ma, H. Dai, Y. Wang, H. Xie, X. Ge, Z. Yang, J. Zhao, W. Hong and Z. Chi, *Aggregate*, 2025, **6**, e70006.
12 S. Lower and M. El-Sayed, *Chem. Rev.*, 1966, **66**, 199–241.
13 G. Baryshnikov, B. Minaev and H. Ågren, *Chem. Rev.*, 2017, **117**, 6500–6537.
14 W. Li, Y. Pan, R. Xiao, Q. Peng, S. Zhang, D. Ma, F. Li, F. Shen, Y. Wang, B. Yang and Y. Ma, *Adv. Funct. Mater.*, 2014, **24**, 1609–1614.
15 W. Shao and J. Kim, *Acc. Chem. Res.*, 2022, **55**, 1573–1585.
16 Y. Liu, L. Gao, X. Zhang, W. Liu, P. Jiang, A. Wang, Z. Wang and Y. Fu, *Aggregate*, 2026, **7**, e70297.
17 R. Yoshii, A. Hirose, K. Tanaka and Y. Chujo, *Chem. – Eur. J.*, 2014, **20**, 8320–8324.
18 R. Yoshii, A. Hirose, K. Tanaka and Y. Chujo, *J. Am. Chem. Soc.*, 2014, **136**, 18131–18139.
19 M. Yamaguchi, S. Ito, A. Hirose, K. Tanaka and Y. Chujo, *J. Mater. Chem. C*, 2016, **4**, 5314–5319.
20 S. Ito, A. Hirose, M. Yamaguchi, K. Tanaka and Y. Chujo, *J. Mater. Chem. C*, 2016, **4**, 5564–5571.
21 S. Ito, K. Tanaka and Y. Chujo, *Inorganics*, 2019, **7**, 100.
22 S. Ito, M. Yaegashi, K. Tanaka and Y. Chujo, *Chem. – Eur. J.*, 2021, **27**, 9302–9312.

23 S. Ito, K. Tanaka and Y. Chujo, *Dalton Trans.*, 2024, **53**, 14858–14865.
24 S. Ito, K. Suwa and K. Tanaka, *Asian J. Org. Chem.*, 2025, **14**, e202500188.
25 S. Ito, T. Hosokai, K. Tanaka and Y. Chujo, *Commun. Chem.*, 2024, **7**, 202.
26 M. Stanoppi and A. Lorbach, *Dalton Trans.*, 2018, **47**, 10394–10398.
27 M. Urban, K. Durka, P. Górka, G. Wiosna-Sałyga, K. Nawara, P. Jankowski and S. Luliński, *Dalton Trans.*, 2019, **48**, 8642–8663.
28 B. C. Garain, P. K. Samanta and S. K. Pati, *J. Phys. Chem. A*, 2021, **125**, 6674–6680.
29 P. H. Marek-Urban, K. A. Urbanowicz, K. Wrochna, P. Pander, A. Blacha-Grzechnik, S. T. Hauer, H. R. V. Berens, K. Woźniak, T. J. J. Müller and K. Durka, *Chem. – Eur. J.*, 2023, **29**, e202300680.
30 J. Adamek, P. H. Marek-Urban, K. Woźniak, K. Durka and S. Luliński, *Chem. Sci.*, 2023, **14**, 12133–12142.
31 M. Urban, K. Wrochna, P. H. Marek-Urban, D. R. Natkowski, K. Woźniak, P. Pander, A. P. Monkman, K. Durka and S. Luliński, *J. Mater. Chem. C*, 2024, **13**, 146–159.
32 S. Ito, M. Hashizume, H. Taka, H. Kita, K. Tanaka and Y. Chujo, *Mater. Chem. Front.*, 2023, **7**, 4971–4983.
33 K. Momma and F. Izumi, *J. Appl. Crystallogr.*, 2011, **44**, 1272–1276.
34 (*a*) CCDC 2529534: Experimental Crystal Structure Determination, 2026, DOI: 10.5517/ccdc.csd.cc2qx5wq; (*b*) CCDC 2529535: Experimental Crystal Structure Determination, 2026, DOI: 10.5517/ccdc.csd.cc2qx5xr; (*c*) CCDC 2529536: Experimental Crystal Structure Determination, 2026, DOI: 10.5517/ccdc.csd.cc2qx5ys; (*d*) CCDC 2529537: Experimental Crystal Structure Determination, 2026, DOI: 10.5517/ccdc.csd.cc2qx5zt; (*e*) CCDC 2529538: Experimental Crystal Structure Determination, 2026, DOI: 10.5517/ccdc.csd.cc2qx60w.